

Singularity of Lévy walks in the lifted Pomeau-Manneville map

Samuel Brevitt*

*Centre for Complex Systems, School of Mathematical Sciences,
Queen Mary University of London, Mile End Road, London E1 4NS, UK*

Alexander Schulz†

Hochschule für Technik und Wirtschaft Dresden, Friedrich-List-Platz 1, 01069 Dresden, Germany

Dominic Pegler‡

*Department of Economics, HKUST Business School, The Hong Kong University
of Science and Technology, Clear Water Bay, Kowloon, W6 8RH, Hong Kong*

Holger Kantz§

Max Planck Institute for the Physics of Complex Systems, Nöthnitzer Straße 38, 01187 Dresden, Germany

Rainer Klages¶

*Centre for Complex Systems, School of Mathematical Sciences,
Queen Mary University of London, Mile End Road, London E1 4NS, United Kingdom and
London Mathematical Laboratory, 8 Margravine Gardens, London W6 8RH, United Kingdom*

(Dated: October 28, 2024)

Since groundbreaking works in the 1980s it is well-known that simple deterministic dynamical systems can display intermittent dynamics and weak chaos leading to anomalous diffusion. A paradigmatic example is the Pomeau-Manneville (PM) map which, suitably lifted onto the whole real line, was shown to generate superdiffusion that can be reproduced by stochastic Lévy walks (LWs). Here we report that this matching only holds for parameter values of the PM map that are of Lebesgue measure zero in its two-dimensional parameter space. This is due to a bifurcation scenario that the map exhibits under variation of one parameter. Constraining this parameter to specific singular values at which the map generates superdiffusion by varying the second one, as has been done in previous literature, we find quantitative deviations between deterministic diffusion and diffusion generated by stochastic LWs in a particular range of parameter values, which cannot be cured by simple LW modifications. We also explore the effect of aging on superdiffusion in the PM map and show that this yields a profound change of the diffusive properties under variation of the aging time, which should be important for experiments. Our findings demonstrate that even in this simplest well-studied setting, a matching of deterministic and stochastic diffusive properties is non-trivial.

Lévy walks are pioneering, very popular models in stochastic theory that have been widely used to understand diffusive spreading in many different fields of science. They provide a basic mechanism to generate anomalous superdiffusion, thus defining a complete different class of stochastic processes compared to normal diffusive Brownian motion. Lévy walks were first applied to understand superdiffusion in a simple weakly chaotic dynamical system that yields a deterministic random walk on the line. Here, we show that this matching between deterministic and stochastic diffusion breaks down for typical values of the two control parameters in the original model. This is due to a bifurcation scenario that defies any mapping onto a simple stochastic process. We also report more subtle quantitative deviations even in the singular case of parameter values where the deterministic system does generate superdiffusion.

I. INTRODUCTION

Diffusion is a fundamental feature of many systems in nature, technology and society [1]. Many diffusive processes, such as Brownian motion, are classically characterised by the mean square displacement (MSD) of a diffusing particle increasing

*Electronic address: s.brevitt@qmul.ac.uk

†Electronic address: alexander.schulz2@htw-dresden.de

‡Electronic address: ecdjpeger@ust.hk

§Electronic address: kantz@pks.mpg.de

¶Electronic address: r.klages@qmul.ac.uk

linearly with time, $\langle x^2 \rangle \sim t$. However it is also more recently observed in many natural processes that the MSD may instead increase as t^β , where β can be lesser (called *subdiffusion*) or greater (*superdiffusion*) than unity (*normal diffusion*). Observations of anomalous diffusion are found in fields as diverse as physics, microbiology, chemistry and finance [2–8].

Independently of this, the development of chaos theory led to an interest in the pseudo-stochastic and diffusive properties of deterministic chaotic dynamical systems [9–15]. The simplest examples are given by deterministically chaotic one dimensional maps, introduced and studied in pioneering works at the beginning of the 1980s [16–18], whose trajectories have a natural relationship to those of random walks. In the decades since, their diffusive dynamics have been explored by many different methods, such as stochastic theory [16–32], periodic orbit theory [33–37], thermodynamic formalism [38, 39] and transfer operator techniques [24, 27, 40, 41]. These maps were found to exhibit many interesting properties, like fractal parameter dependencies of transport coefficients [14, 24, 30, 31, 40], transitions to weak chaos (in terms of sub-exponential separation of trajectories) [42–44] and intermittency (periods of chaos punctuated by periods of laminar flow) [45–47] yielding different types of diffusion, which make them useful models for a variety of systems observed in the natural sciences.

One important class of low-dimensional, time-discrete maps is the Pomeau-Manneville (PM) map, first constructed in order to study the chaos observed in turbulent flows in continuous-time Lorenz systems [45–47]. The map may be defined in its reduced form on the unit interval by

$$x_{n+1} := \tilde{M}(x_n) \quad \text{for} \quad \tilde{M}(x) := x + ax^z \pmod{1} \quad (1)$$

depending on parameters $a > 0$ and $z \geq 1$ for $0 \leq x \leq 1$, where x_n is the position of a point at discrete time $n \in \mathbb{N}$. This map has an unstable marginal fixed point at $x = 0$ which for certain ranges of the nonlinearity parameter z is known to produce intermittency and weak chaos [42, 45]. By imposing symmetry and translation relations, this map can be extended across the real line, to produce a map exhibiting either subdiffusion or superdiffusion by careful positioning of the fixed point [19, 22, 31, 34, 38]; see Sec. II for details.

For the subdiffusive extension of the PM map (1), the time-scaling of the MSD and its dependence on the nonlinearity parameter z have been determined by different methods [19, 22, 23, 26, 29–31, 34–36, 38], as has the associated generalised diffusion coefficient (GDC) [35, 36], which is the multiplicative constant in front of the MSD [5, 31, 44]¹

$$K := \lim_{t \rightarrow \infty} \frac{\langle x^2(t) \rangle}{t^\beta}. \quad (2)$$

Its full dependence on the two control parameters a and z was reported in [30, 31], where computer simulation results were compared with analytic approximations obtained from continuous-time random walk (CTRW) theory. It was shown that under variation of z the GDC becomes zero right at the transition from normal to subdiffusion.

For the superdiffusively extended PM map, similar studies to those above were performed on the special case of parameter values $a = 2^z$, [20–23, 34, 38, 41]. They revealed that as the nonlinearity parameter z increases, the MSD transitions through three different regimes: from normal diffusion ($\beta = 1$) to superdiffusion ($1 < \beta < 2$) to ballistic motion ($\beta = 2$). Most well-known became the groundbreaking works by Geisel et al. [20], and Shlesinger, Zumofen and Klafter [21–23]. They led to the formulation and first application of the *Lévy walk* (LW), a fundamental superdiffusive process in stochastic theory, introduced in parallel purely on the basis of stochastic CTRW theory [48–50]. Due to wide applications across many different fields of science LWs became quite famous and popular over the past few decades; see [8] for a review. The GDC associated to LWs was calculated by CTRW theory [23] and is recovered as a special case from related, more general CTRW walk models studied very recently [51–54]. Note, however, that CTRW theory represents only a stochastic modelling of the map’s original deterministic dynamics by using simplifying assumptions. Hence, in contrast to the calculations in [34, 38, 41] based on methods of dynamical systems theory, applying stochastic LW results to deterministic maps provides no derivation of their diffusive properties from first principles. Furthermore, and for the work presented here most importantly, so far MSD and GDC have only been calculated for parameter values under the constraint $a = 2^z$ for which the PM map exhibits full branches on unit intervals, which in turn generates particularly simple dynamics [24, 27]. Without this constraint, ie., under independent variation of both a and z , the GDC of the superdiffusive PM map has been investigated numerically only very recently [55, 56] and not been calculated analytically. In particular, the well-known stochastic LW results for MSD and GDC have not been compared with results for the PM map under variation of both parameters. References [55, 56] reported preliminary simulation results for the GDC under variation of the nonlinearity z , while [56] focused on the dependence of the GDC related to the parameter a .

Exact analytical results for transport coefficients of dynamical systems, like the GDC, under general parameter variation have been obtained for simple piecewise linear maps (see, eg., [14] for a review). But to our knowledge, there are none for nonlinear dynamical systems like the PM map. A common approach to understand diffusion in these systems is thus to compare

¹ It should be noted that the definition of the GDC in (2) differs from the standard definition of the ‘classical’ diffusion coefficient $D := \lim_{t \rightarrow \infty} \frac{\langle x^2 \rangle}{2t}$ commonly used in physics. Here we apply the convention as defined in (2) as introduced in relation to anomalous diffusion [5].

computer simulation results for the deterministic dynamics with approximations from stochastic theory, as discussed above. This approach, however, is generally non-trivial, since *per se* there is no reason why stochastic modelling should yield exact results for a given deterministic dynamical system. There is a wide range of examples illustrating this difficulty, eg., diffusion generated by simple one-dimensional maps (normal [24], sub- [31] and superdiffusion [55, 56]), nonlinear one-dimensional maps exhibiting bifurcation scenarios [57, 58], two-dimensional standard maps [59], polygonal billiards [14], periodic Lorentz gases [60–62], and soft Lorentz gases [63], to name a few. We furthermore remark that transport coefficients in low-dimensional periodic deterministic dynamical systems typically exhibit fractal parameter dependencies, due to topological instability and periodic orbits [14], which defies a naïve understanding in terms of stochastic theory. Random walk dynamics of these systems is only recovered in certain special [27] or limiting [25] cases of parameter values which allow some mapping onto a Markov process.

Accordingly, in this article we investigate to what extent the MSD of the superdiffusively-extended PM map, considered as a function of its parameters z and a , can be understood in terms of a corresponding stochastic LW model. Our two main results are, first, that the special setting $a = 2^z$, which traditionally has been studied in the literature, is the only one in parameter space that yields dynamics compatible with LWs; and second, that even in this setting, in a certain range of parameter values there are subtle deviations between the GDC calculated from stochastic LW theory and the one obtained numerically from the deterministic PM map. Our paper is organised as follows: After introducing the superdiffusive extension of the PM map at the beginning of Sec. II, we briefly outline the methods used for our numerical analysis (Sec. II A) before we review the corresponding stochastic LW model formulated in terms of CTRW theory (Sec. II B). In Sec. III we describe and discuss the numerical results obtained under variation of a more conveniently chosen parameter related to a , and demonstrate that superdiffusion is only attained for the particular singular parameter values $a = 2^z$, while the dynamics are either normal or localised for others; this is related to a fractal bifurcation scenario, which we investigate in this section. In Sec. IV we give numerical results for the GDC of the map under variation of its nonlinearity parameter z , fixing $a = 2^z$, as has been done before, and compare these to those predicted by LW theory. We provide a detailed analysis of the different diffusive regimes, and the transitions between them, in terms of the GDC. We discover a noteworthy discrepancy between the PM map and LWs in the regime of normal diffusion, which we investigate and partially explain. Finally, in Sec. IV C we explore the effect of aging on the GDC and compare our simulations with recently reported analytic results calculated from an aged LW. We summarise in Sec. V, and discuss some potential physical applications of this work.

II. MODEL AND METHODS

The diffusive extension of the map we consider is given by

$$M(x) = x + R((2x)^z - 1) \quad \text{for } 0 < x < \frac{1}{2} \quad , \quad (3)$$

lifted across the real line by degree one

$$M(-x) = -M(x) \quad \text{and} \quad M(x+1) = M(x) + 1. \quad (4)$$

This version of the map was studied extensively in [56], and is closely related to systems investigated in [22, 23, 34, 38, 55]. The implicit variable prefactor of $a = R2^z$ ensures that M maps $[0, \frac{1}{2}]$ onto $[-R, \frac{1}{2}]$, regardless of z . Therefore, R defines the ‘height’, or the distance outside of the unit box that the map extends [25], which in turn directly parameterizes the size of the ‘coupling regions’ between different boxes (see Fig. 1). At $z = 1$, the map reduces to a piecewise linear map, the dynamics of which are well understood, eg. [14, 24, 25, 27, 64]. Note that this definition of the map moves the function $M(x)$ at integer values, where the original PM map mod 1 has marginal fixed points, outside of the boxes into the coupling regions, which provides a mechanism to potentially generate superdiffusion. Keeping these fixed points outside of the coupling regions within the boxes instead generates subdiffusion [19, 20, 22].

A. Numerical methods

Numerical computation of the MSD $\langle x^2 \rangle$ and the GDC $K(R, z)$ directly from the map is done in two ways: firstly, one may simply sample the MSD from an ensemble of sample trajectories

$$\mathcal{M}(t) := \frac{1}{N} \sum_{i=1}^N \left(x_t^{(i)} - x_0^{(i)} \right)^2 \quad (5)$$

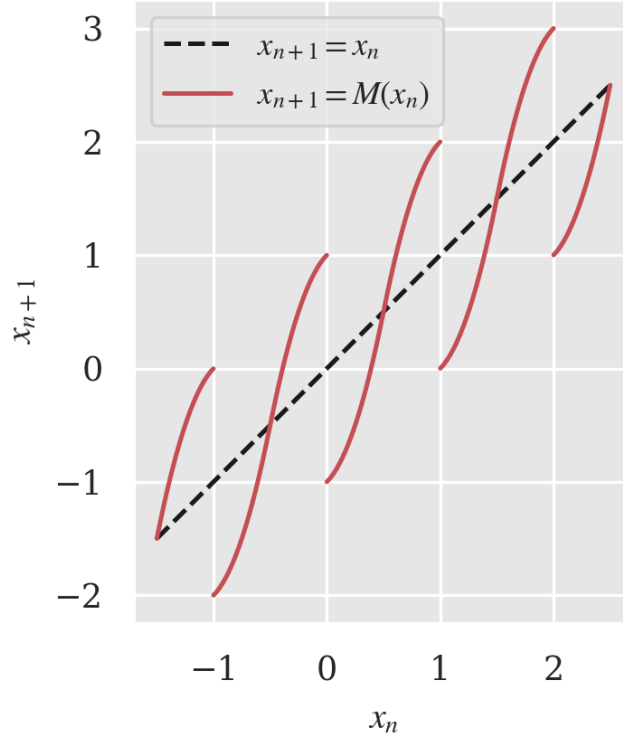


Figure 1: The superdiffusive extension of the Pomeau-Manneville map for the case $z = 2$, $R = 1$ (solid, red online). In black (dashed) is also shown the line $x_{n+1} = x_n$ for comparison.

taking each $x_0^{(i)}$ randomly according to some distribution on the unit interval. Then since we anticipate $\mathcal{M}(t) \sim t^\beta$, we estimate

$$\hat{\beta} = \lim_{i \rightarrow \infty} \frac{\log \mathcal{M}(t_{i+1}) - \log \mathcal{M}(t_i)}{\log(t_{i+1}) - \log t_i} \quad (6)$$

(for a sequence of sampling times t_i to be selected appropriately – here we choose them logarithmically so that the denominator in (6) is constant), from which follows

$$\hat{K}(R, z) = \lim_{t \rightarrow \infty} \frac{\mathcal{M}(t)}{t^{\hat{\beta}}}. \quad (7)$$

This method was used extensively in [56] (which contains further details of the method) and for much of Sec. III in which we study the dependence of these quantities on R . For the variation of z , in Sec. IV, we use the Taylor-Green-Kubo (TGK) formula [12, 65] which expresses the MSD in terms of an exact summation formula over correlations between ‘velocities’ [28, 31, 64, 66] that, in a time-discrete setting, we take as displacements per timestep. We found this approach to be more computationally efficient than other approaches, and a particular advantage is that this summation can also be broken down into its constituent parts to analyse the effects of higher-order correlations, as we will do in Secs. IV and IV B. The method works as follows: by defining

$$v_k := x_{k+1} - x_k \implies x_t - x_0 = \sum_{k=0}^{t-1} v_k$$

we produce the expansion [12, 65]

$$\begin{aligned}
K(z) &= \lim_{t \rightarrow \infty} \frac{1}{t^\beta} \langle (x_t - x_0)^2 \rangle \\
&= \lim_{t \rightarrow \infty} \frac{1}{t^\beta} \sum_{k=0}^{t-1} \sum_{l=0}^{t-1} \langle v_k v_l \rangle \\
&= \lim_{t \rightarrow \infty} \frac{1}{t^\beta} \left[\sum_{k=0}^{t-1} \langle v_k^2 \rangle + 2 \sum_{k=0}^{t-1} \sum_{j=1}^{t-k-1} \langle v_k v_{k+j} \rangle \right]. \tag{8}
\end{aligned}$$

Care must be taken in simplifying this expansion any further, as in our case, unlike in many systems, $\langle v_k v_{k+j} \rangle$ is not necessarily stationary. As is typical [28, 64], we consider only the integer part of each x_k , and neglect the fractional part. This choice eliminates microscopic (within each unit ‘box’) correlations and ensures that the first term can be understood as a simple random walk result that, for the present setting, correctly reproduces the exact value of $K(1) = \frac{2}{3}$, thus giving a physically meaningful ‘lowest order’ approximation [25, 28, 64]. Naturally, for $t \rightarrow \infty$ the same asymptotic result is given by either approach.

In both methods, the MSD and GDC are dependent on taking an ensemble average, the outcome of which may depend strongly on the distribution of initial conditions used in the ensemble (see Sec. IV C for details). For our numerical results in Secs. III and IV we average over an ensemble of simulated trajectories (at least $N = 10^4$), each of which is initialised with x_0 distributed uniformly over the unit interval; in Sec. IV C we consider the case in which the ensemble is ‘aged’ by some initial time t_a , and compare it to the non-aged case below. The physical significance of this is that initial conditions in aged ensembles are in some sense closer to equilibrium conditions, ie. closer to the system’s invariant density, if one exists. In cases where an invariant density does not exist, the aging time parameter is of interest in its own right (see Sec. IV C for details).

B. Predictions for LWs from CTRW theory

Anomalous diffusion in this type of deterministic dynamical system has often been modelled stochastically by CTRWs [19–22, 29–31], a type of random walk in which both the vectors of displacement, and the time interval between displacement events, are drawn randomly from a defined joint distribution; see [2, 4, 5, 8, 67] for reviews. It is well-studied partly due to the rich theory of Montroll and Weiss [68–70], which enables many key statistics such as the MSD to be easily extracted. The classical CTRW approach [20, 22, 23, 30, 31] models the time spent by a particle in the laminar phase of motion near the fixed point of the reduced map as being distributed according to the power law (Pareto Type II, Lomax, or q -exponential² distribution)

$$w(t) = \frac{\gamma b^\gamma}{(b+t)^{1+\gamma}} \tag{9}$$

for $\gamma := 1/(z-1)$ and $b := \gamma/a$. This distribution is generated from the map by the following simplified reasoning [19, 20, 22, 31]: The motion of a particle in the neighbourhood of the fixed point may be modelled as a continuous laminar motion, obeying a differential equation

$$\frac{dx}{dt} \approx x_{n+1} - x_n = ax^z$$

which is easily solved. The time taken to ‘escape’ from the fixed point may be determined from this motion as the time taken to reach $x(t) = 1$ from a given injection point $x(0) = x_0$ [31], and the distribution of escape times follows by assuming a uniform injection density of x_0 .

In the CTRW model (here taken in one dimension only), a particle is initialised at the origin at time $t = 0$, and, for a sequence of time durations t_i drawn i.i.d. from the distribution with density $w(t)$, moves with a constant velocity in a random direction (left or right, with equal probability) for a duration t_i . At the points between time intervals t_i , a new direction is chosen independently. In this sense, the CTRW defines a ‘semi-Markov’ process, in which the displacements at each step are Markov with respect to the step number, but not with respect to the physical system time. Details of how this method is applied to our case are given in Appendix A, and for further details of this method see references [8, 22, 23, 31, 55, 67].

² under the parameter change $\gamma = \frac{2-q}{q-1}$, for $1 < q < 2$ [71]

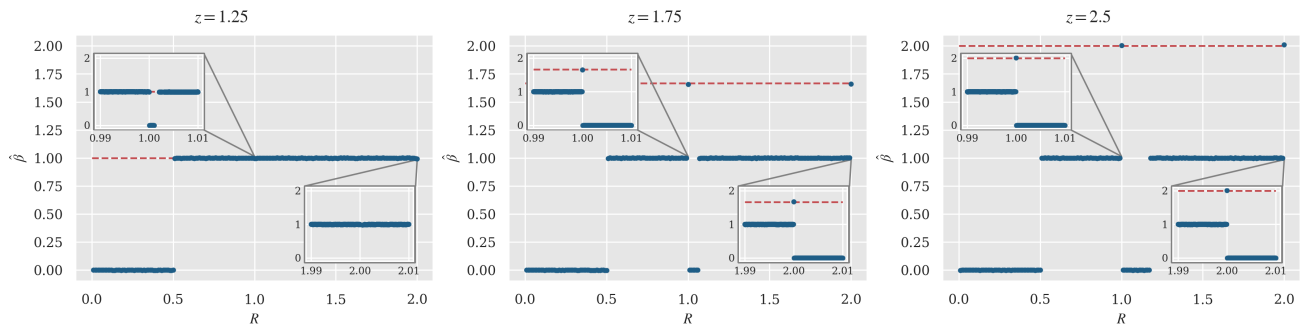


Figure 2: Numerically computed $\hat{\beta}(R, z)$ for $z \in \{1.25, 1.75, 2.5\}$ (from top), computed from an ensemble of $N = 10^5$ initially uniformly distributed sample trajectories aged by $T_a = 10^6$ timesteps. Main figures are computed for 201 values of $R \in [0, 2]$ ($\Delta R = 0.01$); insets are computed with 201 values each of $R \in [0.99, 1.01]$ and $R \in [1.99, 2.01]$ respectively ($\Delta R = 10^{-4}$). Dashed lines (in red) indicate predictions given by CTRW theory in (11).

Using the CTRW defined above gives the MSD of what is called a LW [21–23, 48–50] to leading order as

$$\langle x^2 \rangle \sim v_0^2 \begin{cases} \frac{2b}{\gamma-2} t, & 1 < z < \frac{3}{2}, \\ \frac{2b^{\gamma-1}(\gamma-1)}{(3-\gamma)(2-\gamma)} t^{3-\gamma}, & \frac{3}{2} < z < 2, \\ (1-\gamma) t^2, & z > 2. \end{cases}$$

The time-dependence on t^β is very well known [20, 22, 23, 26, 29–31, 34–36, 38]. The multiplicative constant yielding the GDC was first reported in [23], more recently within the context of higher-dimensional LWs in the supplemental material of [51], and in the context of generalised LWs with non-constant velocity in [52, 53]; we discuss this quantity in more detail in Sec. IV C.

We see from the generated formulae that the parameter space of z is divided into three distinct regimes, corresponding to three phases of $\beta(z)$, at the boundaries of which $K(z)$ either vanishes or blows up: (I) where $1 < z < \frac{3}{2}$, for which the diffusion is normal ($\beta = 1$); (II) where $\frac{3}{2} < z < 2$, for which superdiffusion is observed ($1 < \beta < 2$); and (III) where $z > 2$, for which an extreme form of superdiffusion, dominated by ballistic motion, is observed ($\beta = 2$). These emerge from the CTRW calculations as a direct result of moments of the jump time distribution $w(t)$ ceasing to exist due to heavy tails: in (I), where $\gamma > 2$, $w(t)$ has a well-defined mean and variance and so the Central Limit Theorem dictates the diffusion to be normal and with (in the long time limit) a Gaussian propagator; in (II), $1 < \gamma < 2$ and therefore $w(t)$ has a first moment but not a second, resulting in anomalous diffusion; in (III), $0 < \gamma < 1$ and therefore not even a first moment exists for $w(t)$, resulting in ballistic trajectories of unbounded average length.

III. VARIATION OF COUPLING LENGTH R

A. On the diffusive exponent β

In this section, we review the diffusive behaviour of the map (3) in terms of β , under variation of the coupling length R . We show that, away from the nicely understood special case $R = 1$, the quantity β is highly non-trivially dependent on R ; we find that superdiffusion is only attained for some very specific values, and diffusion is completely suppressed in others. For these purposes we fix $z \in \{1.25, 1.75, 2.5\}$, thus exploring typical behaviours in each of the map’s three main dynamical regimes.

Results from numerical simulations for the quantity $\hat{\beta}$ are shown in Fig. 2. From this we draw the following conclusions:

For all z , if $R \leq \frac{1}{2}$, then trivially $\beta = 0$, since all unit boxes $[k - \frac{1}{2}, k + \frac{1}{2}]$, $k \in \mathbb{Z}$ are positively invariant, and therefore the dynamics are completely localised. For $z = 1$, for all other $R > \frac{1}{2}$, the dynamics are normally diffusive ($\beta = 1$; cf. [14, 24, 25, 27, 64]).

For $z > 1$, if $R \in \mathbb{N}$, then we attain the superdiffusion described in Sec. II B. This is possible because in this case, the map’s marginal point maps onto a copy of itself, displaced by R steps to the left or to the right. This allows for extended ‘runs’ in one direction or the other, generating superdiffusion [20, 22]. For *most* other values $R \notin \mathbb{N}$, however, the diffusion is normal; since if the marginal point of M does not map onto itself, all higher iterates of the map M^2, M^3, \dots are uniformly hyperbolic.

However, for $z > 1$, there is not always normal diffusion when $R \notin \mathbb{N}$: we observe intervals of the form $R \in (\ell, \ell + \delta_c]$, $\ell \in \mathbb{N}$, $\delta_c = \delta_c(R, z)$ in which β completely vanishes. This is because if x_0 is in a neighbourhood of the origin, then $M(x_0)$, rather than mapping onto a neighbouring branch pointing in the same direction, as in superdiffusion, instead maps onto the reverse branch, so that $M^2(x_0)$ is returned once again to the origin, see Fig. 3(a). Under these conditions, it is possible for there to exist some

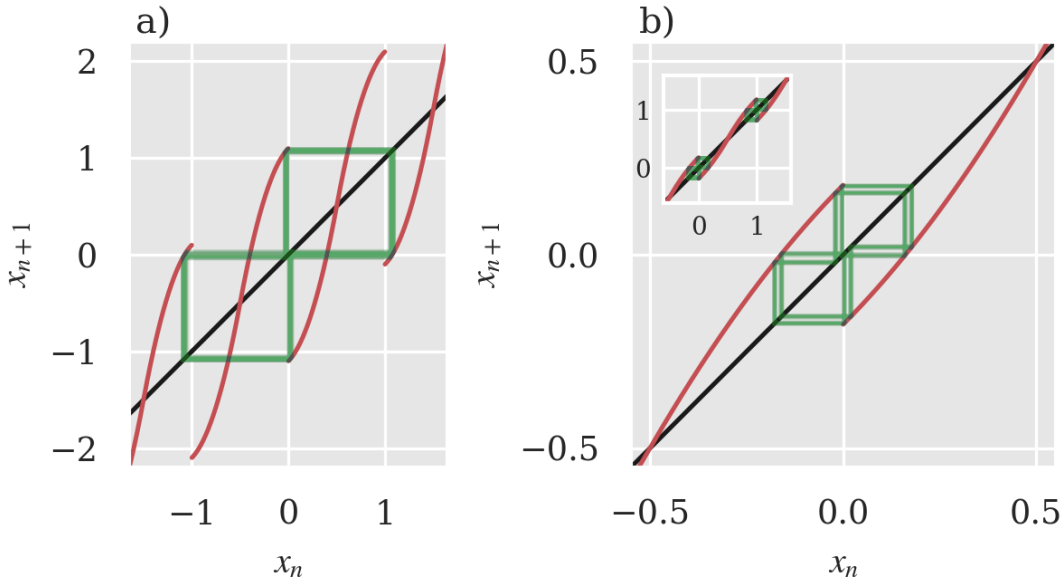


Figure 3: Cobweb plots showing two examples of special invariant sets. (a) The region $[-x_c, x_c]$ is invariant under M^2 in the map with $z = 2$, $R = 1.1$, causing $\beta = 0$. (b) Orbits in the map with $z = 2$, $R = 0.18$ localise around four disconnected intervals, close to $x \in \mathbb{Z}$, producing the bifurcation in Fig. 4.

$x_c(R)$ such that $M^2([-x_c, x_c]) \subseteq [-x_c, x_c]$, therefore causing the dynamics to remain localised. Finally, since the remainder of the map is repelling, almost all trajectories are eventually absorbed into this localisation cycle. On the other hand, if $R > k + \delta_c$, such a x_c may not exist, and normal diffusion is returned.

Let us denote the ranges of R where diffusion is suppressed in this way by

$$\mathcal{N}_k(z) := \{R \in (k, k + 1] : \beta(R, z) = 0\}, \quad k \in \mathbb{N}. \quad (10)$$

Trivially $\mathcal{N}_0(z) = (0, \frac{1}{2}]$ as remarked above. However, we also now see that for $z > 1$ and $k \geq 1$, zero-sets exist of the form $\mathcal{N}_k(z) = (k, k + \delta_c]$. Based on our limited numerical evidence, we suggest the following claims: if μ is the Lebesgue measure,

1. $\mu(\mathcal{N}_{k+1}(z)) < \mu(\mathcal{N}_k(z))$ (zero-sets get smaller as we increase k);
2. $\mu(\mathcal{N}_k(z)) < \mu(\mathcal{N}_k(z'))$ if $z < z'$ (zero-sets get larger as we increase z).

As z increases, the fixed point becomes ‘stickier’, thus widening the range of R for which x_c can exist; conversely, for larger k , the expanding gradient of the map is larger, reducing the marginal point’s stickiness.

In conclusion, we see that, far from the idealised picture presented by the well-studied $R = 1$ scenario, there is instead a wide range of diffusive behaviours that can be observed, including normal diffusion and localisation, of which superdiffusion is a rare special case. Further, we note that β is highly discontinuous in R , meaning that superdiffusion is not dynamically stable to small perturbations of the map (cf. [72]). One may now wonder about the functional form of the associated GDC under variation of R and z , which has been studied numerically in [56]. As is already well-known from previous works on parameter-dependent diffusion in simple one-dimensional maps, whenever diffusion is normal for the PM map the GDC appears to be a fractal function of R ; see [14] for a review and [24, 25, 27] for the special case $z = 1$. Whenever there are localisation regions with $\hat{\beta} = 0$ the GDC jumps to zero while superdiffusive parameter values of R correspond to local maxima in the GDC. How precisely these transitions happen in terms of continuity properties of the GDC as a function of R remains an interesting open question, as this is very difficult to resolve in computer simulations. Similar transitions to localisation regions related to bifurcation scenarios have been reported in [57, 58] for a nonlinear and in [40] for a biased piecewise linear map.

B. Bifurcation scenario

Further, in this section we explore a complex bifurcation scenario that the map undergoes under transition of $R \in \mathcal{N}_k(z)$. In this region, the map’s dynamics are localised, causing $\beta = 0$; we examine this localisation to reveal a detailed fractal bifurcation

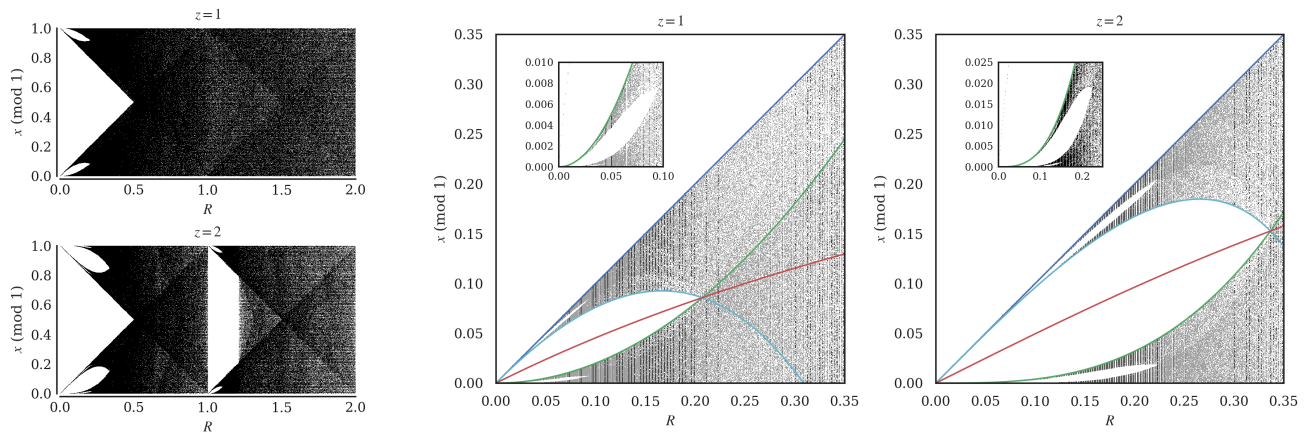


Figure 4: Left: Orbits of the map $M(x) \pmod{1}$ (3), for $N = 10^3$ sample trajectories running for $T = 10^7$ timesteps, for 2×10^3 values of $R \in [0, 2]$ ($\Delta R = 10^{-3}$), for $z \in \{1, 2\}$ (from top). Observe the complex bifurcation scenario that is present for small R , and the qualitative difference observed under change of z . Center and right: Zoomed portions of left, in comparison with the dynamic contours mentioned in the text, and calculated in the appendix: the boundary of M given by R in blue; the boundaries of M^2 , namely x_α and x_β , in green and cyan respectively; and the unstable fixed point x_u of M^2 in red. The contours of M^2 collide at the critical point R_c , see text. Insets show a further zoomed portion indicating an iterative hierarchy of bubble-like structures.

structure. In order to assess this in the nonlinear PM map, we first examine it as it manifests in the linear map when $z = 1$.

In Fig. 4 are shown stable orbits, modulo 1, of the Pomeau-Manneville map $M(R, z)$ under continuous variation of R , for $z \in \{1, 2\}$. (These values of z are chosen for ease of calculation.) In cases where we have normal diffusion we have (strong) chaos (in the sense of positive Lyapunov exponents), and these orbits cover the entire unit interval. However, as noted earlier, when $R \in \mathcal{N}_k(z)$, orbits are localised to particular subregions of the state space. For $z = 1$, the stable regions are, by trivial inspection of the map (see Fig. 3(b) inset, for example) $\bigcup_{j \in \mathbb{Z}} [j - R, j + R]$. At $x = j + \frac{1}{2}$, $j \in \mathbb{Z}$, the map has a repelling (unstable) fixed point. At $R = \frac{1}{2}$, the boundaries of the stable sets connect with each other *and* coincide with the unstable fixed point, at which point normal diffusion is achieved. In bifurcation theory, this marks a crisis point [73]. As discussed above, for $z > 1$ we see a repetition of this bifurcation when $R = k + \delta$, $k \in \mathbb{N}$, as R passes through $\mathcal{N}_k(z)$, after which normal diffusion is abruptly restored at some point R_d . The exact point at which this occurs is calculated analytically in Appendix B, for the case $z = 2$, and we believe this may coincide with the end of $\mathcal{N}_k(z)$; i.e., normal diffusion is restored once all areas of phase space, in particular the repelling area, are reachable, see Fig. 9 in the Appendix.

However, we see that this is not the full bifurcation picture. Analysing the map's second iterate M^2 , we find another bubble-like region in the interval $[0, R]$, and symmetrically in $[-R, 0]$ (appearing in Fig. 4 as $[1 - R, 1]$), dividing the stable orbits into two smaller disjointed intervals. As can be seen from the map, this is due to two further unstable fixed points of M^2 (unstable periodic points of M) appearing in these regions. At some critical value R_c , the boundaries of these regions coincide, and the two regions merge. This separation manifests as a 'bubble' in the left-most corners of the plots in Fig. 4; the centre and right plots in that figure show close-up images of these regions.

In the cases $z = 1$ and $z = 2$ we are able to calculate exactly the dynamical boundaries of these stable regions, which we denote by $x_\alpha(R)$ and $x_\beta(R)$, see Fig. 4. In Appendix B, we calculate exact values of $x_\alpha(R)$ and $x_\beta(R)$, and the unstable periodic point $x_u(R)$, analytically, and deduce the point R_c at which it is shown they coincide. These three critical quantities are shown as coloured curves on Fig. 4. Further, we see in these figures (see insets) that these subregions divide further for smaller R , creating another hierarchy of bubbles, the boundaries of which are determined by the third iterate M^3 of the map. (In Fig. 3(b) this third-order bubble can be seen quite clearly separating the stable orbits shown.) We conjecture that this hierarchy of bubbles is infinite, producing a fractal bifurcation structure; in Fig. 10 in the Appendix we show a series of zoomed-in plots for a range of values of z depicting increasingly higher orders of this structure. This result should be viewed in the light of known bifurcation structures in other, similar diffusive maps, such as the climbing sine [57, 58]. and a biased piecewise linear map [40].

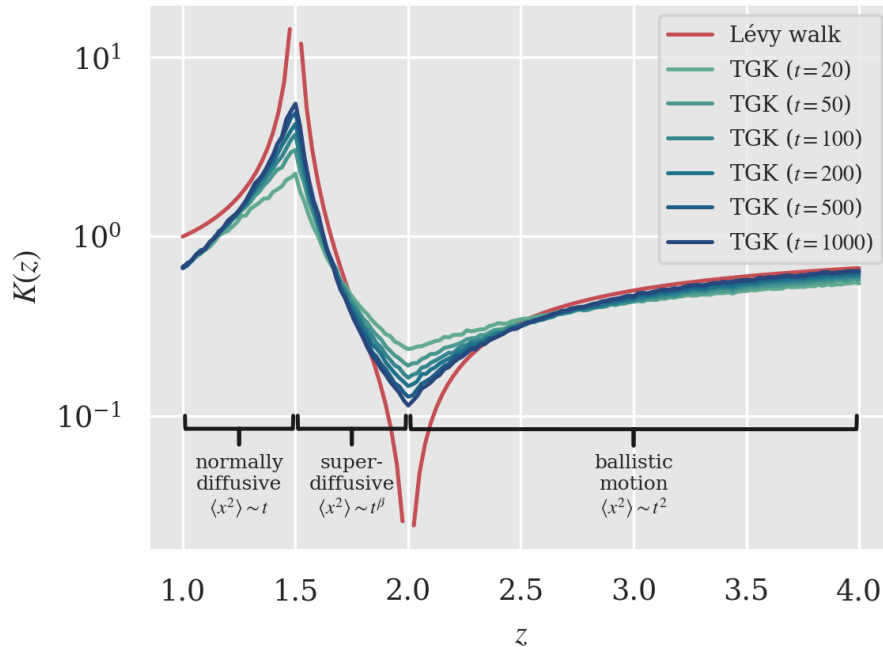


Figure 5: The GDC $K(z)$ (2) generated from TGK expansions (8) of the superdiffusive PM map (3), using increasingly many terms t of the expansion and the analytic estimate for β obtained from (11) (rough curves, t increasing from light to dark). Also shown is the LW approximation taken from (11) and (2) (smooth curve, red online). The different dynamical regimes shown in (11) are annotated on the plotting area. All plots are generated from an ensemble of 10^4 simulated trajectories and consist of 151 points.

IV. VARIATION OF NONLINEARITY z

A. Results

Using the CTRW defined in Sec. II B gives the MSD of the LW to leading order as $a = 2^z$, [20–23, 34, 38, 41]

$$\langle x^2 \rangle \sim v_0^2 \begin{cases} \frac{2b}{\gamma-2} t, & 1 < z < \frac{3}{2}, \\ \frac{2b^{\gamma-1}(\gamma-1)}{(3-\gamma)(2-\gamma)} t^{3-\gamma}, & \frac{3}{2} < z < 2, \\ (1-\gamma) t^2, & z > 2, \end{cases} \quad (11)$$

for v_0 a velocity term; in the case $R = 1$, whereby near the fixed point a particle is displaced one unit per timestep, we set $v_0 = 1$; although not commonly studied, via the same reasoning we may take for other $R \in \mathbb{N}$ the same formulae, substituting $v_0 = R$ appropriately. These results are shown in Fig. 5, along with numerical estimates of the same quantity calculated via the TGK formula in (8), as described in Sec. II. The numerics are seen to generally fit well to the formulae, notwithstanding a few remarks which we discuss below:

At the dynamical transition points $z = \frac{3}{2}$ and $z = 2$, we observe in the case of the LW that $K(z)$ approaches infinity and zero respectively. This is because, considering a more detailed expansion, via the same methodology [20, 22], at the transition points between dynamical regimes, logarithmic corrections to the MSD cause the GDC to be ill-defined at the transition points,

$$\langle x^2 \rangle \sim \begin{cases} t \log t, & z = \frac{3}{2}, \\ t^2 / \log t, & z = 2, \end{cases} \quad (12)$$

which matches to exact results for the PM map obtained by methods of dynamical system theory [34, 38, 41]. Fig. 5 shows that around these two transition points $K(z)$ displays characteristic shapes. Numerical estimates with finite computation time cannot overcome the slow logarithmic corrections of (12) to reproduce these analytical predictions accurately; but taking increasingly many terms t from the TGK expansion (which equates to looking at the process over a longer time) indeed produces sharper peaks and troughs at the dynamic transitions (see Fig. 5), thus confirming convergence to the LW scenario at least qualitatively.

We observe a clear convergence in regime (III) when $z > 2$ of the numerical GDC towards the curve generated from the LW from below (in Sec. IV C, we reveal we also have convergence from above). Likewise, our numerical study indicates good general matching and a promising convergence to the LW result in regime (II) for $\frac{3}{2} < z < 2$. However, for regime (I) where $0 < z < \frac{3}{2}$ we notice a significant discrepancy, which relates to the limit of $K(z)$ as $z \rightarrow 1$. It is given by the stochastic LW calculations as $K(1) = 1$, but is shown numerically to have the value approximately $\frac{2}{3}$. Since for $z = 1$ the function $M(x)$ reduces to a linear shift map, the true value can also be calculated via straightforward analytic means to be $K(1) = \frac{2}{3}$, matching to a simple random walk result [24, 25, 27, 28, 64]. This represents a major problem with the CTRW calculations which, to the knowledge of the authors, does not appear to be mentioned or explained in any existing literature, which instead typically treats the CTRW as an accurate representation of the map's dynamics. We attempt to give our analysis of this discrepancy below.

B. Understanding the discrepancy between deterministic dynamics and CTRW theory

That there should be such a discrepancy is not *per se* surprising, since it was also shown in the subdiffusive case that in the regime of normal diffusion, for $z < \frac{3}{2}$, the Lévy model is invalid and instead a selectively constructed random walk was used to match $K(z)$ in this parameter region [31]. A normally-diffusive CTRW with exponential waiting times was also applied and found to match sufficiently well in this regime [31]. In the superdiffusive case however we were unable to identify any natural parameters of the system to fit an exponential walk process to match the numerical results.

The reason for this is as follows: consider the distribution from which the time durations t_i (described in Sec. II) are drawn. For the parameters $z < \frac{3}{2}$ we assume (based on both numerical and CTRW-derived evidence) this distribution has at least its first two moments, ie. $\mathbb{E}[t_i] = \mu_1 < \infty$ and $\mathbb{E}[t_i^2] = \mu_2 < \infty$. This allows us to write the Laplace transform of the density function (cf. Sec. II B, calculations in Appendix A, and [31]) as

$$\tilde{w}(s) = 1 - \mu_1 s + \frac{\mu_2}{2} s^2 + \mathcal{O}(s^3), \quad (13)$$

from which we can derive via the same Montroll-Weiss theory

$$\langle x^2 \rangle(t) \simeq \frac{\mu_2}{\mu_1} t + o(t), \quad (14)$$

implying $K(z) = \mu_2/\mu_1$. While there are plenty of distributions which can reproduce the correct limit of $K(z) = \frac{2}{3}$ at $z = 1$ (eg. an exponential distribution with rate $\lambda = 3$), one would still have to motivate from first principles why these parameters are justified, based on the dynamics of the map. Further, to obtain the distinct phase transition at $z = \frac{3}{2}$, these parameters would also have to undergo a transition which, again, must be dynamically motivated (eg., we would require $\lambda \rightarrow 0$ as $z \rightarrow \frac{3}{2}$ for an exponential distribution, etc.).

In general, and in stark contrast to the corresponding subdiffusive case, we expect that an exponential or Dirac-like CTRW (whose dynamics would generate a simple random walk) will be unable to reproduce the behaviour of $K(z)$ for $z < \frac{3}{2}$, due to high-order correlations which appear in the map's dynamics for *all* $z > 1$, and not only those near the $z = \frac{3}{2}$ limit. These are obtained from the decomposition of the TGK series described in Sec. II. In Fig. 6 we show this decomposition, with a fixed time parameter of $t = 200$, in the region $1 < z < \frac{3}{2}$, as a series of increasing partial expansions, starting with the '0th'-order expansion – comprising only the first of the two terms in (8) – and sequentially adding cross-correlations from the second term of the formula (we call the '*m*th'-order expansion that in which j is allowed to range from 1 to m ; ie., correlations between displacements up to m time units apart are considered). This decomposition reveals the immediate presence of high-order correlations between timesteps in the map's dynamics, which precludes the modelling of the process as a random walk. Only in the $z = 1$ limit is the correct GDC obtained if in the TGK expansion we do not consider correlation terms (in which case, as is already known, the map can be modelled simply by a random walk).

In principle the incorporation of correlations derived from a TGK-type expansion into a random walk model could lead to a suitable representation of the dynamics as a higher-order Markov process, a correlated random walk, or some other such process. However the above investigation reveals to us that as $z \rightarrow \frac{3}{2}$, the required order of correlations under consideration becomes very large. This indicates to us that the transition between normal diffusion and superdiffusion in this regime represents a highly non-trivial dynamical scenario, much more so than its subdiffusive counterpart. This transition scenario corresponds to the immediate realisation of the marginal fixed point which is present for all $z > 1$, and causes the map to no longer be hyperbolic. In [74] it was shown that for the PM map, this transition guarantees a rate of escape from the fixed point which is asymptotically a power law for all $z > 1$. In the case $z = 1$, on the other hand, this distribution becomes exponential.

We observe this transition scenario in Fig. 7, which shows the discrepancy between the density $w(t)$, prescribed by CTRW, for the time between displacement events, and the density of the true number of timesteps a random point (injected uniformly) on the PM map (3) will take until it leaves the branch containing the marginal fixed point, determined numerically by iteratively calculating preimages of the escape point on the marginal branch of the map. We notice that, for $z > 1$, $w(t)$ is indeed asymptotic

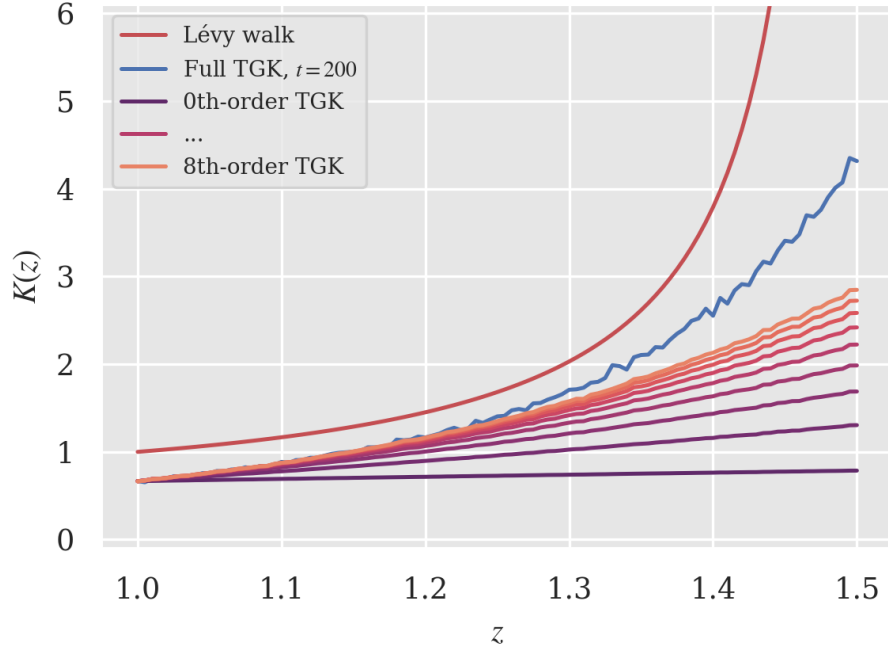


Figure 6: $K(z)$ generated from TGK expansions (8) of the superdiffusive PM map, using increasingly many orders of correlation terms $\langle v_k v_{k+j} \rangle$ (lower rough curves, m increasing from dark to light). Also shown are the LW approximation (11) (uppermost smooth curve, red online) and the full TGK expansion (uppermost rough curve, blue online). All TGK plots are taken using 200 terms of a TGK expansion from an ensemble of 10^4 simulated trajectories and consist of 101 points.

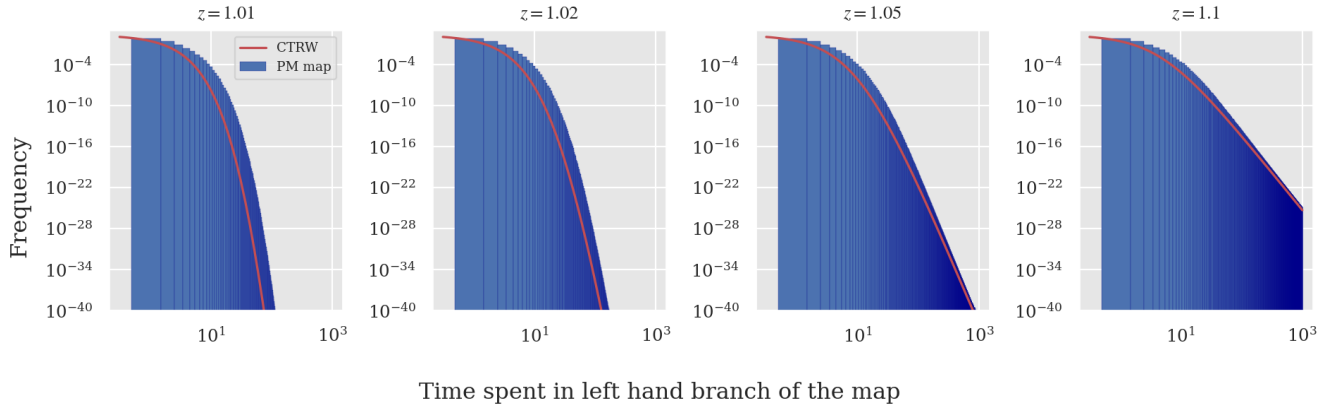


Figure 7: Histograms of the time spent in the left-hand branch (adjacent to the marginal point) of the PM map, calculated from pre-iterates of the map, for varying values of z . In red for comparison is shown the corresponding density $w(t)$ as prescribed by (9). Backwards iterates from the map are generated using numerical root finding using Python's `decimal` package, to 40 decimal places.

to the 'true' density, with only a transient difference, but this difference grows unboundedly in scale and in duration in the limit $z \rightarrow 1$, eventually spanning many orders of magnitude. Similar transients were noted in relation to power laws in, eg., [75] and references therein, and can lead to poor or misleading statistics for a variety of chaotic systems. This may also be a contributing factor to the difference observed in the GDC.

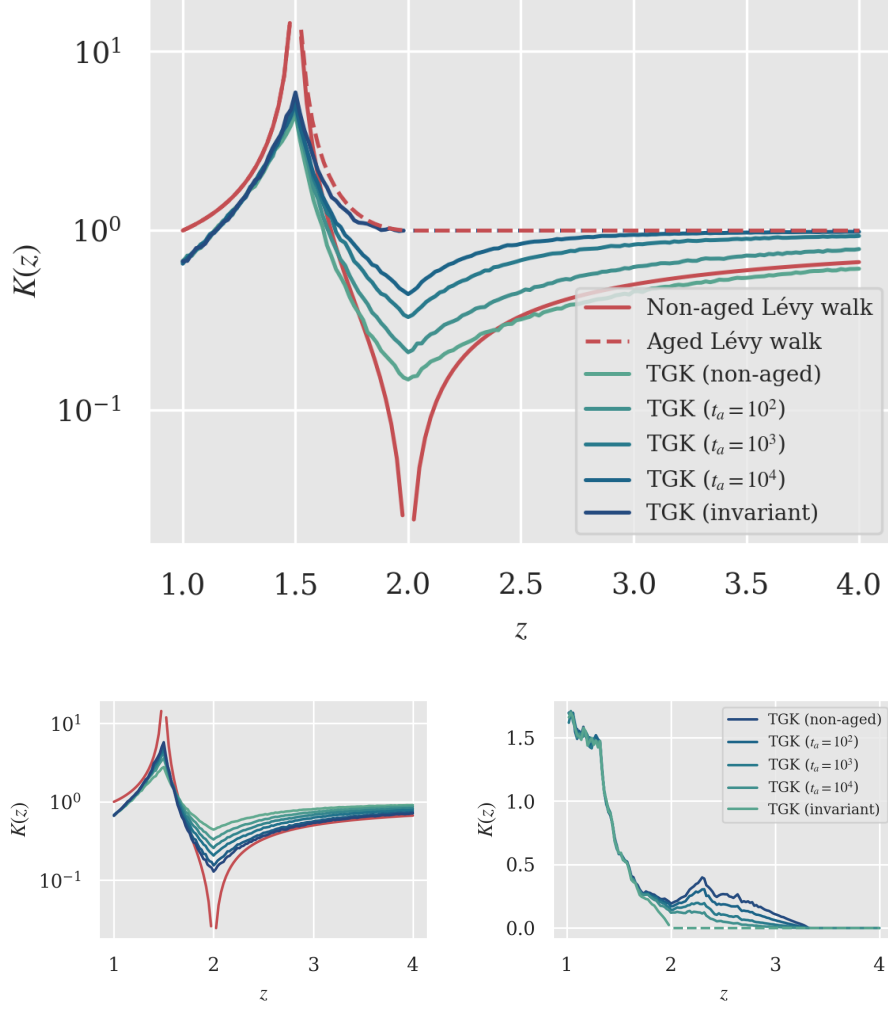


Figure 8: Top: TGK approximations of $K(z)$ for the superdiffusive PM map, starting from increasingly aged ensembles of particles initialised from a uniform density (aging duration increasing from light to dark), as well as starting from a normalisable invariant density (where it exists; darkest uppermost curve, blue online). Also shown are the results for the non-aged LW discussed above (smooth curve, red online) and the aged LW discussed in [52, 53] (dashed line, top, red online). All TGK plots are taken using 200 terms of a TGK expansion from an ensemble of 10^4 simulated trajectories and consist of 151 points (50 points in the case of the invariant ensemble). Bottom left: an identical plot to that shown in Fig. 5, but with points initialised from an ensemble aged by 100 timesteps. Bottom right: an identical plot to that shown above, for the subdiffusive extension of the map studied in [31], mirroring Fig. 7 in that paper, with $\alpha = 5$ fixed (aging duration increasing from dark to light, invariant curve shown at the bottom, in teal online).

C. Effect of aging on the generalised diffusion coefficient

Finally, we explore the consequences of aging on numerical estimates of $K(z)$. In the present setting, aging denotes the dependence of the MSD, and hence of $K(z)$, on the duration, or aging time, between the initialisation of the system dynamics and the start of its measurement [29, 76–79]. Up to this point all estimates have been taken commencing from a uniform density of $\{x_0\}$. However, many systems observed in nature typically evolve for a long time before human measurement of them can commence, and therefore we also consider the case where we allow a degree of relaxation towards the invariant density to take place before beginning measurements. We denote the number of timesteps during which the system is allowed to evolve before measurement begins as the ‘aging time’ t_a . In such cases it is known that the dynamics of systems exhibiting aging are characteristically dependent on the ratio of measurement time to aging time, t/t_a [78].

In Fig. 8 we apply varying degrees of aging to an ensemble of trajectories before calculating $K(z)$ via a numerical TGK expansion. We also show the same calculations starting from the (approximate) invariant density where it exists for $z < 2$; inspired by [78, 80–83], which show the invariant density of the reduced map (1) to be asymptotic to $\tilde{\rho}(x) \propto x^{1-z}$, we initialise

our points from

$$\tilde{\rho}(x) \propto x^{1-z} + (1-x)^{1-z}. \quad (15)$$

For $z \geq 2$ the only normalisable invariant density is the delta function on $\{0, 1\}$, which implies almost all particles undergo purely ballistic motion in a single direction. Also shown is the corresponding analytic result for a LW in the limit of large aging relative to measurement time, $t/t_a \ll 1$, as a special case of recently reported results in [53]. It is known that the MSD of aged walks corresponds exactly to the ensemble-averaged time-averaged MSD, with the averaging time equated to the aging time t_a [54]. In [53] this was calculated for a generalised LW with non-constant velocity, of which our stochastic model is merely a special case.

The non-aged GDC from simulations is identical to that shown in Fig. 5. As the aging time increases, the GDC from the aged ensemble converges uniformly both to the GDC from the ensemble initialised on the invariant density, where it exists (as the aged ensemble converges to the invariant one), and to the aged LW results in [53], shown in red. While for $z < \frac{3}{2}$ in regime (I) the GDC is not visibly affected by the aging, for $z > \frac{3}{2}$ in regimes (II) and (III) the qualitative effect of aging is easily observed – most notably, where in the non-aged scenario the dynamic transition at $z = 2$ was marked by a total vanishing of the GDC, aging seems to wipe out this phenomenon completely, and the limit of small t/t_a does not exhibit any at all of the logarithmic corrections discussed previously at $z = 2$ which cause $K(z)$ to vanish.

The cause of this effect – the uniform raising of the $K(z)$ curve visible for $z > \frac{3}{2}$ – may be due to the fact that the aged densities feature a more concentrated accumulation near the marginal points $\{0, 1\}$, which would lead to increased correlations in the short term as more particles are in the ballistic phase of motion. The disappearance of logarithmic corrections at $z = 2$ may be explained by the limiting density converging to the delta function at the point of transition, resulting in $K(z) \approx 1$. Only once the measurement time greatly exceeds and dominates over the aging time will the regular results be recovered [53, 78].

That there is no effect of aging on $K(z)$ in regime (I) for $z < \frac{3}{2}$ is to be expected, since in this regime, any initial density converges to the invariant one in exponential time. In contrast, it is known that for $z \geq 2$ the PM map is only weakly ergodic [6, 78], and therefore undergoes dynamical aging [31, 78, 80, 81]. Interestingly though, some aging is observed on $K(z)$ even in the intermediate superdiffusive regime (II), $\frac{3}{2} < z < 2$, in which a normalisable invariant density still exists. This reflects what was described for LWs as ‘ultra-weak’ ergodicity breaking in that parameter regime, which is characterised by a deviation in the GDC, but not the exponent, of the time dependence of the MSD [84–86].

A similar effect is observed for subdiffusive dynamics. In the bottom right inset of Fig. 8 is shown an equivalent plot showing the GDC for the subdiffusive PM map used in [31], with $a = 5$, mirroring Fig. 7 in [31]. The same phenomenon as in the superdiffusive case is observed: above $z > \frac{3}{2}$, aging begins to uniformly reduce $K(z)$ until it converges to the result from the invariant density, which in this case is $K(z) = 0$ for $z > 2$.

Incidentally, it was also observed in [30, 31] that for the subdiffusive map, there is strong numerical evidence that the exact form of the GDC has a dependence on the map’s parameter which is fractal in nature, in contrast to the smooth function generated by the LW; see Fig. 8 (bottom right) for an example. It is already long known that fractal diffusion coefficients are in fact quite typical for many classes of deterministic dynamical systems [14, 30, 31, 58, 87]. Although we do not conclude here whether or not this is true of the superdiffusive extension given here, under variation of z , the possibility cannot be excluded, which further precludes an intimate comparison equating the map’s dynamics to those of the stochastic model.

We conclude this section by presenting a general principle: that, for measurements taken over finite time, we believe it is (perhaps counterintuitively) preferable to average one’s ensembles over a uniform initial density than from one closer to the more ‘natural’ invariant density. This is especially evident in those regimes (II) and (III) for which $z > \frac{3}{2}$, in which the map’s ergodicity is broken. We see that, this way, results from a uniform initial density in practice better reproduce the curve seen in the long measurement time limit, without simulations becoming dominated by effects introduced by aging; and for short sampling times, measuring from an aged or even invariant density can produce perverse results which are not representative of the long-measurement-time GDC of the process. Our exposition here supplies some numerical evidence to back this principle.

V. CONCLUSION

In this article we conducted an analysis on a superdiffusive extension of the PM map. We calculated numerically the MSD exponent $\beta(R, z)$ and GDC $K(R, z)$ of the map, as a function of the parameter of the map’s nonlinearity z , and its coupling length R , using both direct simulations and TGK expansions, and compared these findings to a well-known CTRW model in the form of a LW which models the map’s dynamics stochastically in an important special case. Within this special case $R = 1$, the LW model reproduces the numerically calculated $K(z)$ well for some values of the parameter z , but suffers a systematic and previously unexplained and unaddressed quantitative deviation in the limit of normal diffusion $z \rightarrow 1$. In this region a deeper investigation reveals the dynamics are highly non-trivial, in a much more subtle way than in the case of the corresponding subdiffusive extension. Outside of this special case, the diffusive dynamics of the map do not follow a LW, and indeed are shown not to be superdiffusive at all, but instead are normally diffusive except in a few key regions of the dual parameter space (K, z) in

which diffusion is totally suppressed, due to dynamics becoming localised. Under variation of these parameters in these regions, the dynamics undergo a complex bifurcation scenario generating a fractal structure of stable regions in phase space, which is produced numerically for the first time and the contours of which are, to some extent, analytically calculated.

We also investigated the effect of aging on our numerical findings. We find, in accordance with recently reported results, that in the limit of increased aging time t_a/t , the suppression of $K(z)$ at the transition from superdiffusion to ballistic motion is eliminated, for finite measurement times, while the divergence at the other, from normal to superdiffusion, is preserved. This elimination is also reproduced in the case of the subdiffusive PM map. We identify this as a problem of conflicting limits as both aging time and measurement time go to infinity, which requires one to take caution when conducting numerical or even physical experiments. We state a general principle that uniform initial densities should be preferred in simulations to more ‘natural’ invariant ones if the ergodicity of the dynamics is not ensured, a claim which is supported numerically.

In summary, our results illustrate again the subtlety to understand diffusion generated by deterministic dynamical systems on the basis of simple stochastic models that are applied *ad hoc* to a given dynamical system. Often it seems taken for granted that the dynamics of a ‘sufficiently chaotic’ deterministic model boils down to a more simplistic random walk-type process. Our analysis demonstrates, first of all, that the celebrated matching of deterministic superdiffusion in the lifted PM map to stochastic LWs only applies to a very specific, singular subset of parameter values in the full parameter space. In other words, the diffusive dynamics of this model turns out to be highly unstable under parameter variation, affected by an underlying basic bifurcation scenario. Secondly, for specific parameter values where the map exhibits superdiffusion, as predicted by stochastic LW theory, the parameter dependence of the GDC can indeed to a large extent, *but by no means completely*, be understood in terms of LWs generated by CTRW theory. This shows that in general one may have to dig deeper in order to achieve a complete understanding of the original deterministic dynamics. These results may cast some doubt on the ubiquity of LWs in deterministic dynamical systems and may be relevant when investigating more realistic systems modeled by, for example, nonlinear deterministic equations of motion.

Correspondingly, it would be very interesting to test whether dynamical transitions in the GDC, and associated aging effects, can be observed in experiments. As candidates we would be thinking of blinking quantum dots and cold atoms in atomic lattices, where features of anomalous diffusion, aging, and weak ergodicity breaking have already been reported [88]. It would also be worthwhile to explore theoretically the parameter dependence of generalised transport coefficients in other types of anomalous dynamical systems, such as stochastic generalised Langevin dynamics [3] and weakly chaotic models like polygonal billiards and related systems [14], which are known to generate a variety of different dynamical transitions. From a mathematical angle, it is also an interesting open question as to whether the fractal nature of the map’s bifurcation structure under variation of R can be proven formally and not only shown numerically, for this and other related classes of diffusive maps.

Appendix

A. CTRW calculations

In the superdiffusive extension of the map, the marginal point is mapped one unit to the left or to the right (see Fig. 1), and therefore in the CTRW model the time spent in the neighbourhood of the marginal point is equated exactly with time spent in a ballistic motion with constant velocity v_0 (we take $v_0 \equiv 1$) [21, 22],

$$p(\ell | t) = \frac{1}{2} \delta(|\ell| - v_0 t), \quad (16)$$

where we enable the particle to move either left or right along a one-dimensional axis with equal probability. These choices define the model as a LW [8, 48–50]. From (9) and (16) the joint density

$$\psi(x, t) = w(t) p(x | t)$$

follows.

Under these assumptions, one may obtain the appropriate Montroll-Weiss equation [8, 22, 67],

$$\hat{P}(k, s) = \text{Re} \left\{ \frac{1 - \tilde{w}(s + iv_0 k)}{s + iv_0 k} \right\} \frac{1}{1 - \hat{\psi}(k, s)},$$

where $P(x, t)$ is the spatial density of the random walker as a function of time, and (k, s) are the respective Fourier- and Laplace-transformed variables for (x, t) (such transformations are henceforth indicated by $\hat{}$ and $\tilde{}$ respectively). The Laplace-transformed MSD can then be found very easily by

$$\langle \tilde{x}^2(s) \rangle = \left. \frac{\partial^2}{\partial k^2} \hat{P}(k, s) \right|_{k=0} \quad (17)$$

to which an inverse transform may be performed to obtain $\langle x^2 \rangle(t)$. Frequently such inverse transforms are intractable and instead we rely on asymptotic analysis as $(k, s) \rightarrow (0, 0)$ to obtain the desired quantities to the required order. The GDC [5, 30, 31] can then be defined by

$$K(z) := \lim_{t \rightarrow \infty} \frac{\langle x^2 \rangle}{t^\beta} \quad (18)$$

for the appropriate $\beta > 0$ wherever this limit exists, and is finite and non-zero.

B. Bifurcation calculations

We restrict our discussion to the interval $[-\frac{1}{2}, \frac{1}{2}]$. Let $M^+(x)$ and $M^-(x)$ denote the variants of the map to be applied when x is positive or negative respectively, ie., from (3),

$$\begin{aligned} M^+(x) &= x + R((2x)^z - 1), \\ M^-(x) &= -M^+(-x) \\ &= x - R((-2x)^z - 1), \end{aligned}$$

which for $z = 1$ reduces to

$$\begin{aligned} M^+(x) &= x + 2Rx - R, \\ M^-(x) &= x + 2Rx + R, \end{aligned}$$

and for $z = 2$

$$\begin{aligned} M^+(x) &= x + 4Rx^2 - R, \\ M^-(x) &= x - 4Rx^2 + R. \end{aligned}$$

For $z = 1$, it is apparent by inspection that the box onto which the dynamics are localised is given by

$$[M^+(0), M^-(0)] = [-R, R].$$

Therefore let us restrict ourselves further to the interval $[-R, R]$. Inspecting M^2 , we identify an invariant region at $[-x_\alpha, x_\alpha]$ with

$$\begin{aligned} x_\alpha &= M^+(M^-(0)) \\ &= (x + 2Rx + R) + 2R(x + 2Rx + R) - R|_{x=0} \\ &= x(1 + 4R + 4R^2) + 2R^2|_{x=0} \\ &= 2R^2 \end{aligned}$$

and at $[-R, -x_\beta] \cup [x_\beta, R]$ with

$$\begin{aligned} x_\beta &= M^2(-R) = M^-(M^-(-R)) \\ &= (x + 2Rx + R) + 2R(x + 2Rx + R) + R|_{x=-R} \\ &= x(1 + 4R + 4R^2) + 2R^2 + 2R|_{x=-R} \\ &= R - 2R^2 - 4R^3. \end{aligned}$$

The unstable fixed point $x_u > 0$ (and identically $-x_u < 0$) appears when $M^2(x_u) = M^-(M^+(x_u)) = x_u$, ie.

$$\begin{aligned} (x_u + 2Rx_u - R) + 2R(x_u + 2Rx_u - R) + R &= x_u \\ \implies x_u(1 + 4R + 4R^2) - 2R^2 &= x_u \\ \implies x_u(4R + 4R^2) &= 2R^2 \\ \implies x_u &= \frac{R^2}{2R(1 + R)}. \end{aligned}$$

It can be shown that all three points coincide at R_c given by the sole positive real solution to the cubic equation

$$\begin{aligned} R_c - 4R_c^2 - 4R_c^3 &= 0 \\ \implies R_c &= -\frac{1}{2} + \sqrt{\frac{1}{2}} \approx 0.207, \\ x_c = x(R_c) &= \frac{3}{2} - \sqrt{2} \approx 0.0858. \end{aligned}$$

For $z = 2$, let us pre-calculate

$$\begin{aligned} (x - 4Rx^2 + R)^2 &= x^2 + 16R^2x^4 + R^2 \\ &\quad - 8Rx^3 + 2Rx - 8R^2x^2 \end{aligned}$$

which gives

$$\begin{aligned} (x - 4Rx^2 + R)^2 \Big|_{x=0} &= R^2; \\ (x - 4Rx^2 + R)^2 \Big|_{x=-R} &= 16R^6. \end{aligned}$$

Then we calculate

$$\begin{aligned} x_\alpha &= M^+(M^-(0)) \\ &= (x - 4Rx^2 + R) + 4R(x - 4Rx^2 + R)^2 - R \Big|_{x=0} \\ &= (x - 4Rx^2 + R) + 4R[R^2] - R \Big|_{x=0} \\ &= 4R^3 \end{aligned}$$

and

$$\begin{aligned} x_\beta &= M^2(-R) = M^-(M^-(-R)) \\ &= (x - 4Rx^2 + R) - 4R(x - 4Rx^2 + R)^2 + R \Big|_{x=-R} \\ &= (x - 4Rx^2 + R) - 4R[16R^6] + R \Big|_{x=-R} \\ &= R - 4R^3 - 64R^7. \end{aligned}$$

Then $x_u > 0$ appears at $M^2(x_u) = M^-(M^+(x_u)) = x_u$, ie.

$$\begin{aligned} (x_u + 4Rx_u^2 - R) - 4R(x_u + 4Rx_u^2 - R)^2 + R &= x_u \\ \implies (-64R^3)x_u^4 + (-32R^2)x_u^3 + (32R^3)x_u^2 \\ &\quad + (8R^2)x_u + (-4R^3 - R) = 0 \\ \implies x_u &= \frac{-1 + \sqrt{1 + 4R^2}}{4R}. \end{aligned}$$

Note that x_u is the solution of a quartic equation whose coefficients vary in R ; hence for increasing z these quantities become very difficult to calculate by hand. The critical point R_c at which these coincide is given by the sole real positive solution to a polynomial equation of degree 7, which we solve here only numerically:

$$\begin{aligned} R_c - 8R_c^3 - 64R_c^7 &= 0 \\ \implies R_c &\approx 0.337, \\ x_c &\approx 0.153. \end{aligned}$$

Extending these calculations to higher, or to non-integer, values of z would undoubtedly lead to quite unwieldy equations, hence values of $z \in \{1, 2\}$ were selected here, although the qualitative dynamics can be seen numerically to be similar.

In Fig. 9, we see that the repelling region of phase space becomes accessible when the branch edge (located near $x_n = 0$) exceeds the critical point x_d , which is a (mod 1) repelling fixed point. In the full map, this is the point where $M(x) = x \pm 1$. Precisely, when $z = 2$, this is the point

$$\begin{aligned} M^+(x_d) &= x_d + 4Rx_d^2 - R = x_d - 1 \\ \implies x_d &= \sqrt{\frac{R-1}{4R}}. \end{aligned}$$

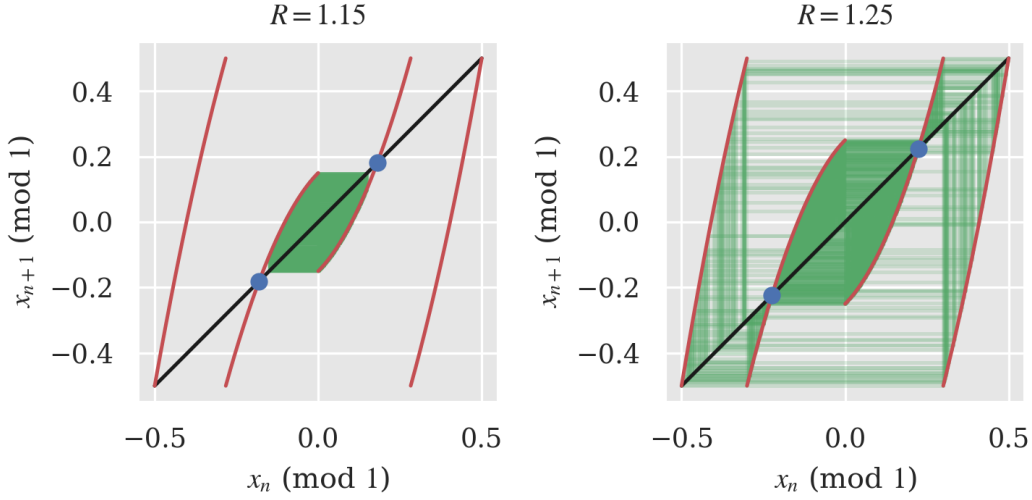


Figure 9: Plots of sample trajectories in the Pomeau-Manneville map (mod 1), over the region $[-\frac{1}{2}, \frac{1}{2}]$, for $z = 2$, $R \in \{1.15, 1.25\}$. The repelling region of the phase space becomes accessible as R exceeds $R_d \approx 1.207$, see text. The critical points $\pm x_d$ are shown in blue.

The critical value R_d is the value of R at which $M^-(0) - 1$ first exceeds x_d , ie.,

$$\begin{aligned} M^-(0) - 1 &= R_d - 1 = \sqrt{\frac{R_d - 1}{4R_d}} = x_d \\ \implies 4R_d^2 - 4R_d + 1 &= 0 \\ \implies R_d &= \frac{1 + \sqrt{2}}{2} \approx 1.207. \end{aligned}$$

Note that this is remarkably close to, but does not quite fit with, the numerically identified values for $\mathcal{N}_1(z)$ (the values of R at which normal diffusion is restored) depicted in Fig. 2. Whether this is due to artefacts in the numerical simulations, or to something more subtle dynamically, remains an open question.

-
- [1] A. Bunde, J. Caro, J. Kärger, and G. Vogl, eds., *Diffusive Spreading in Nature, Technology and Society* (Springer, Berlin, 2018).
 - [2] J. Bouchaud and A. Georges, *Phys. Rep.* **195**, 127 (1990).
 - [3] W. Coffey, Y. P. Kalmykov, and J. T. Waldron, *The Langevin Equation* (World Scientific, Singapore, 2004).
 - [4] R. Klages, G. Radons, and I. M. Sokolov, eds., *Anomalous transport: Foundations and Applications* (Wiley-VCH, Berlin, 2008).
 - [5] R. Metzler and J. Klafter, *Phys. Rep.* **339**, 1 (2000).
 - [6] R. Metzler, J.-H. Jeon, A. Cherstvy, and E. Barkai, *Phys. Chem. Chem. Phys.* **16**, 24128 (2014).
 - [7] F. Höfling and T. Franosch, *Rep. Prog. Phys.* **76**, 046602/1 (2013).
 - [8] V. Zaburdaev, S. Denisov, and J. Klafter, *Rev. Mod. Phys.* **87**, 483 (2015).
 - [9] D. Evans and G. Morriss, *Statistical mechanics of nonequilibrium liquids* (Academic Press, London, 1990).
 - [10] W. Hoover, *Time reversibility, computer simulation, and chaos* (World Scientific, Singapore, 1999).
 - [11] P. Gaspard, *Chaos, scattering and statistical mechanics* (Cambridge University Press, Cambridge, UK, 1998).
 - [12] J. R. Dorfman, *An introduction to chaos in nonequilibrium statistical mechanics*, Cambridge Lecture Notes in Physics No. 14 (Cambridge University Press, Cambridge, UK, 1999).
 - [13] G. Zaslavsky, *Phys. Rep.* **371**, 461 (2002).
 - [14] R. Klages, *Microscopic chaos, fractals and transport in nonequilibrium statistical mechanics*, Advanced Series in Nonlinear Dynamics No. 24 (World Scientific, Singapore, 2007).
 - [15] P. Castiglione, M. Falcioni, A. Lesne, and A. Vulpiani, *Chaos and Coarse Graining in Statistical Mechanics* (Cambridge University Press, Cambridge, 2008).
 - [16] H. Fujisaka and S. Grossmann, *Z. Physik B* **48**, 261 (1982).

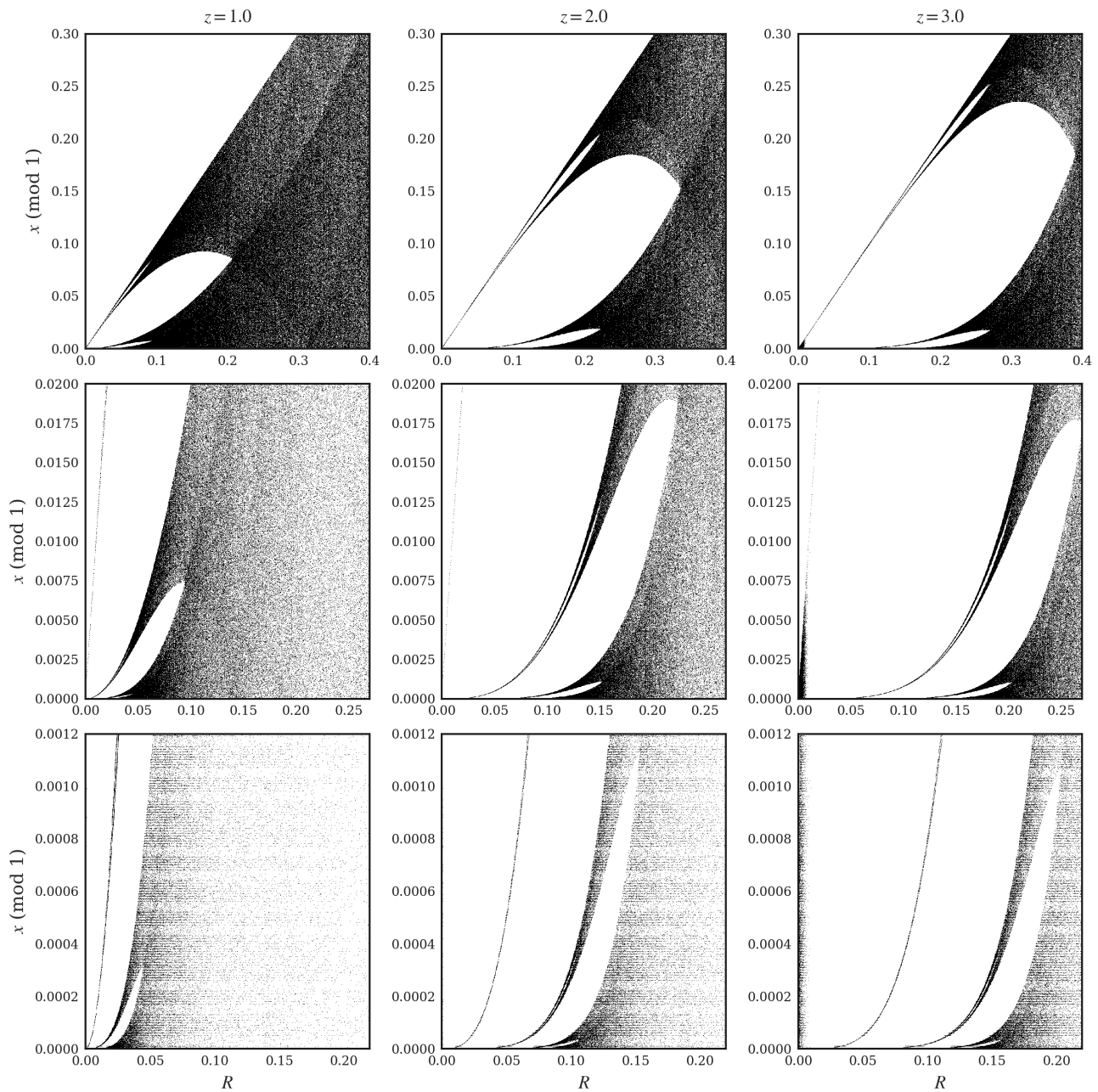


Figure 10: Zooms of Fig. 4 for $z \in \{1, 2, 3\}$ (left to right), for three varying levels of zooming (top to bottom), indicating the hierarchy of bubble-like structures in the neighbourhood of $R = 0, x = 0$. We conjecture this hierarchy to be infinite.

- [17] M. Schell, S. Fraser, and R. Kapral, *Phys. Rev. A* **26**, 504 (1982).
- [18] T. Geisel and J. Nierwetberg, *Phys. Rev. Lett.* **48**, 7 (1982).
- [19] T. Geisel and S. Thomaes, *Phys. Rev. Lett.* **52**, 1936 (1984).
- [20] T. Geisel, J. Nierwetberg, and A. Zacherl, *Phys. Rev. Lett.* **54**, 616 (1985).
- [21] M. Shlesinger and J. Klafter, *Phys. Rev. Lett.* **54**, 2551 (1985).
- [22] G. Zumofen and J. Klafter, *Phys. Rev. E* **47**, 851 (1993).
- [23] G. Zumofen and J. Klafter, *Physica D* **69**, 436 (1993).
- [24] R. Klages and J. R. Dorfman, *Phys. Rev. Lett.* **74**, 387 (1995).
- [25] R. Klages and J. Dorfman, *Phys. Rev. E* **55**, R1247 (1997).
- [26] E. Barkai and J. Klafter, *Phys. Rev. Lett.* **79**, 2245 (1997).
- [27] R. Klages and J. R. Dorfman, *Phys. Rev. E* **59**, 5361 (1999).
- [28] R. Klages and N. Korabel, *J. Phys. A* **35**, 4823 (2002).

- [29] E. Barkai, Phys. Rev. Lett. **90**, 104101/1 (2003).
- [30] N. Korabel, A. Chechkin, R. Klages, I. Sokolov, and V. Gonchar, Europhys. Lett. **70**, 63 (2005).
- [31] N. Korabel, R. Klages, A. Chechkin, I. Sokolov, and V. Gonchar, Phys. Rev. E **75**, 036213 (2007).
- [32] T. Albers, D. Müller-Bender, L. Hille, and G. Radons, Phys. Rev. Lett. **128**, 074101 (2022).
- [33] R. Artuso, Phys. Lett. A **160**, 528 (1991).
- [34] R. Artuso, G. Casati, and R. Lombardi, Phys. Rev. Lett. **71**, 62 (1993).
- [35] C. Dettmann and P. Cvitanovic, Phys. Rev. E **56**, 6687 (1997).
- [36] C. Dettmann and P. Dahlqvist, Phys. Rev. E **57**, 5303 (1998).
- [37] P. Cvitanović, R. Artuso, R. Mainieri, G. Tanner, and G. Vattay, *Chaos: Classical and quantum* (Niels Bohr Institute, Copenhagen, 2007) webbook under chaosbook.org.
- [38] X.-J. Wang and C.-K. Hu, Phys. Rev. E **48**, 728 (1993).
- [39] R. Stoop, W.-H. Steeb, and G. Radons, Phys. Lett. A **202**, 195 (1995).
- [40] J. Groeneveld and R. Klages, J. Stat. Phys. **109**, 821 (2002).
- [41] S. Tasaki and P. Gaspard, Physica D **187**, 51 (2004).
- [42] P. Gaspard and X.-J. Wang, Proc. Natl. Acad. Sci. USA **85**, 4591 (1988).
- [43] G. Zaslavsky and D. Usikov, *Weak chaos and quasi-regular patterns*, Cambridge Nonlinear Science Series (Cambridge University Press, Cambridge, 2001).
- [44] R. Klages, in *From Hamiltonian chaos to complex systems*, edited by X. Leoncini and M. Leonetti (Springer, Berlin, 2013) pp. 3–42.
- [45] P. Manneville and Y. Pomeau, Phys. Lett. A **75**, 1 (1979).
- [46] P. Manneville, J. Phys. France **41**, 1235 (1980).
- [47] Y. Pomeau and P. Manneville, Commun. Math. Phys. **74**, 189 (1980).
- [48] M. Shlesinger, J. Klafter, and Y. Wong, J. Stat. Phys. **27**, 499 (1982).
- [49] J. Klafter, A. Blumen, and M. Shlesinger, Phys. Rev. A **35**, 3081 (1987).
- [50] M. Shlesinger, B. West, and J. Klafter, Phys. Rev. Lett. **58**, 1100 (1987).
- [51] V. Zaburdaev, I. Fouxon, S. Denisov, and E. Barkai, Phys. Rev. Lett. **117**, 270601 (2016).
- [52] T. Albers and G. Radons, Phys. Rev. Lett. **120**, 104501 (2018).
- [53] T. Albers and G. Radons, Phys. Rev. E **105**, 014113 (2022).
- [54] M. Bothe, F. Sagues, and I. Sokolov, Phys. Rev. E **100**, 012117 (2019).
- [55] D. Pegler, *Anomalous diffusion in weakly chaotic systems*, Master's thesis, Queen Mary, University of London, London, UK (2017).
- [56] A. Schulz, *Parameter-dependent deterministic diffusion in intermittent Pomeau-Manneville maps*, Master's thesis, Technische Universität Dresden, Dresden, Germany (2020).
- [57] N. Korabel and R. Klages, Phys. Rev. Lett. **89**, 214102 (2002).
- [58] N. Korabel and R. Klages, Physica D **187**, 66 (2004).
- [59] A. Rechester and R. White, Phys. Rev. Lett. **44**, 1586 (1980).
- [60] J. Machta and R. Zwanzig, Phys. Rev. Lett. **50**, 1959 (1983).
- [61] R. Klages and C. Dellago, J. Stat. Phys. **101**, 145 (2000).
- [62] T. Gilbert and D. P. Sanders, J. Phys. A: Math. Theor. **43**, 035001/1 (2010).
- [63] R. Klages, S. Gallegos, J. Solanpää, M. Sarvilahti, and E. Räsänen, Phys. Rev. Lett. **122**, 064102 (2019).
- [64] R. Klages, *Deterministic diffusion in one-dimensional chaotic dynamical systems*, Doctoral thesis, Technische Universität Berlin, Berlin, Germany (1995).
- [65] R. Kubo, Rep. Prog. Phys. **29**, 255 (1966).
- [66] G. Knight and R. Klages, Phys. Rev. E **84**, 041135/1 (2011).
- [67] J. Klafter and I. Sokolov, *First steps in random walks: from tools to applications* (Oxford University Press, New York, 2011).
- [68] E. Montroll and G. Weiss, J. Math. Phys. **6**, 167 (1965).
- [69] E. Montroll and H. Scher, J. Stat. Phys. **9**, 101 (1973).
- [70] H. Scher and E. Montroll, Phys. Rev. B **12**, 2455 (1975).
- [71] S. Picoli Jr., R. Mendes, L. Malacarne, and R. Santos, Brazilian Journal of Physics **39**, 468 (2009).
- [72] G. Knight and R. Klages, Phys. Rev. E **84**, 041135 (2011).
- [73] E. Ott, *Chaos in dynamical systems* (Cambridge University Press, Cambridge, UK, 1993).
- [74] M. Demers and B. Fernandez, Trans. Am. Math. Soc. **368**, 4907 (2016).
- [75] P. Dahlqvist, Phys. Rev. E **60**, 6639 (1999).
- [76] J. Bouchaud, J. Phys. I **2**, 1705 (1992).
- [77] E. Barkai and G. Margolin, Israel Journal of Chemistry **44**, 353 (2004).
- [78] T. Akimoto and E. Barkai, Phys. Rev. E **87**, 032915 (2013).
- [79] R. Metzler, J.-H. Jeon, A. G. Cherstvy, and E. Barkai, Phys. Chem. Chem. Phys. **16**, 24128 (2014).
- [80] M. Thaler, Israel Journal of Mathematics **46**, 67 (1983).
- [81] R. Zweimüller, Nonlinearity **11**, 1263 (1998).
- [82] M. Thaler, Studia Mathematica **143**, 103 (2000).
- [83] N. Korabel and E. Barkai, Phys. Rev. E **82**, 016209 (2010).
- [84] R. Metzler, J.-H. Jeon, A. G. Cherstvy, and E. Barkai, Phys. Chem. Chem. Phys. **16**, 24128 (2014).
- [85] D. Froemberg and E. Barkai, Eur. Phys. J. B **86**, 331 (2013).
- [86] D. Froemberg and E. Barkai, Phys. Rev. E **87**, 030104(R) (2013).
- [87] Z. Koza, J. Phys. A **37**, 10859 (2004).
- [88] F. Stefani, J. Hoogenboom, and E. Barkai, Phys. Tod. **62**, 34 (2009).